ELSEVIER

Thermochimica Acta 317 (1998) 7–23

thermochimica acta

Precipitation kinetics in solutionized aluminum alloy 2124: Determination by scanning and isothermal calorimetry

George W. Smith*

Physics and Physical Chemistry Department, General Motors Research and Development Center, Warren, MI 48090-9055, USA

Received 12 September 1997; received in revised form 9 February 1998; accepted 5 April 1998

Abstract

Kinetics and energetics of precipitation in solutionized (SOL) aluminum alloy 2124 have been determined by differential scanning calorimetry (DSC) and differential isothermal calorimetry (DIC). DSC experiments at several temperature scan rates were analyzed by the Kissinger method to give activation energies and rate constants. From the DIC experiments, we obtained kinetics information using a 2-exponential fit, a rate-averaged time constant, and (for GP formation) an Avrami model. It appears that the 2-exponential fit is applicable when two distinct processes contribute to precipitation, while the rate-averaged time constant is appropriate when one process is dominant. Criteria are established for choosing the proper analysis.

Activation energies and time constants from DSC and DIC agree fairly well for both GP zone formation and precipitation. Kinetics results for GP zone dissolution in SOL 2124 were obtainable only from DSC experiments. Both calorimetric methods indicate that, after GP zones have formed and dissolved, two mechanisms are involved in precipitation. The results are compared to DSC studies of other workers for similar alloys. TEM studies indicate that the two precipitation mechanisms in alloy 2124 involve formation of S' ($CuMgAl_2$) and θ' ($CuAl_2$) phases. ΔQ, the heat evolved during GP zone formation and precipitation, was measured isothermally over the 30–300°C range. At the temperature of maximum GP zone formation rate (~70°C), $\Delta Q \approx -14.7$ J/g; at the precipitation maximum (~270°C) $\Delta Q \approx -27.2$ J/g. © 1998 Elsevier Science B.V.

Keywords: Differential isothermal calorimetry; Differential scanning calorimetry; Kissinger analysis; Precipitation kinetics; Solutionized aluminum alloy 2124

1. Introduction

Precipitation in aluminum alloys has been studied by numerous investigators [1–23] using differential scanning calorimetry (DSC). Several analytical schemes have been advanced for determination of kinetic parameters from the scan-rate dependence of peaks observed in DSC curves [24–28]. Two review articles examine these and related analysis methods in detail [29,30].

Differential isothermal calorimetry (DIC) has also been applied, but to a lesser extent [19,31–33]. Recently, we used both DSC and DIC to determine precipitation kinetics and energetics in air-cooled (ACO) aluminum alloy 339 [33]. Scanning results were analyzed by a modified Kissinger equation [24,28] which gave activation energies, E_{act}, for comparison with values from Arrhenius plots of isothermal precipitation time constants. We showed that the Kissinger analysis of the DSC scans gave good agreement with the DIC results, provided the DSC temperature scan rates were slow compared to the reciprocal of the time for the calorimeter to equilibrate [33].

*Corresponding author. Tel.: +1 810 986 0614; fax: +1 810 986 3091; e-mail: george-w.-smith@notes.gmr.com

PII S0040-6031(98)00361-X

In this publication, we extend the DSC analysis of Ref. [33] to a system in which the calorimetry of precipitation is more complex: solutionized/water-quenched aluminum alloy 2124. For this alloy GP zone formation and dissolution as well as two precipitation processes are observed. Nevertheless, it will be seen that when appropriate analyses are used, the two calorimetric methods agree fairly well, suggesting that our methods of analysis are reasonably general. One of the goals of the present work is to develop criteria for choosing the best method to analyze DIC data in cases where either one or two precipitation mechanisms are dominant. Since this is the first publication devoted to validating these methods for a solutionized alloy, we shall present our results in some detail. Comparisons will be made with prior DSC studies of related alloys.

2. Experimental

2.1. Samples and sample treatment

The 2124 aluminum alloy, which contains ∼4.5% Cu, ∼1.6% Mg, and ∼0.1% Si (weight percentages), was fabricated by powder metallurgy techniques, followed by heating and extrusion. Solutionized (SOL) samples were prepared in the following manner: Rods of square cross section were cut from the original material and machined to cylinders with a diameter of 6 mm. Thin slices (∼1.6 mm thick) were then cut for the calorimetric studies (masses ranged from 116 to 132 mg). After machining, the samples were solutionized at 495°C for 1 h, quenched in water and immediately stored in a cold chamber at −74°C for up to 20 days. In order to minimize GP zone formation prior to a DSC or DIC experiment, the samples were weighed and transferred to the calorimeter after only one or two minutes at ambient temperature [34]. The calorimeter reference material was a pure aluminum disk, comparable in mass to the alloy samples.

2.2. Calorimetric methods

Kinetics and energetics of precipitation were determined using Perkin–Elmer DSC2 and DSC7 differential scanning calorimeters, as described previously [33]. The DSC7 instrument was used in its temperature-scanning mode and the DSC2 in its isothermal mode. Scanning experiments reveal exothermic precipitation peaks as well as endothermic dissolution peaks which occur over relatively broad temperature ranges. Detailed information regarding the rate of heat release during precipitation is obtained from a series of isothermal measurements at several temperatures.

2.2.1. Differential scanning calorimetry (DSC)

In the scanning mode the DSC instrument measures the dependence of dQ/dt, the rate of heat absorption or emission by the sample, on temperature T. The position of the baseline in such a plot is proportional to the specific heat of the sample. The area of any endothermic or exothermic peaks superimposed on the baseline is proportional to ΔQ, the heat absorbed or released by the sample, and also to dT/dt, the temperature scan rate. It was previously demonstrated [33] for ACO alloy 339 that, in order to apply the Kissinger analysis, the ratio of the scan rate to the DSC peak width should be less than or comparable to the time for the calorimeter to equilibrate (the lag time, τ_{lag}). This same restriction will be seen to apply to the present work.

Typical DSC scans for SOL alloy 2124 at different scan rates are shown in Fig. 1 and exhibit exotherms due to GP zone formation and precipitation. Values of ΔQ derived for these DSC peaks are approximate because of the interference of two endotherms: one due to GP zone dissolution (between the GP zone formation and precipitation exotherms) and the other to dissolution of precipitates (commencing at temperatures above the precipitation regime). Because of the interference of these endotherms, ΔQ values determined by isothermal calorimetry are more accurate.

2.2.2. Differential isothermal calorimetry (DIC)

Operated isothermally, the calorimeter measures dQ/dt vs. time at a specific temperature. In a typical DIC experiment, the sample temperature is increased rapidly (320°C/min) from −73°C to the desired temperature. During the first 30–60 s after that temperature is reached, the data are invalid due to non-equilibrium sample conditions; this short interval roughly defines τ_{lag} [33]. Techniques to correct for

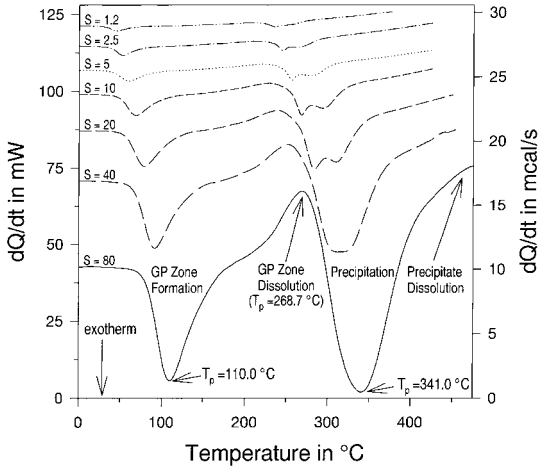

Fig. 1. Plots of dQ/dt vs. temperature for solutionized alloy 2124 run at scan rates, S, ranging from 1.2 to 80°C/min. The low temperature exothermic peak for each scan is due to GP zone formation. Two precipitation exotherms at high T are resolved for S<40°C/min but coalesce at higher scan rates. In each scan, an endotherm due to GP dissolution is seen just below the precipitation exotherm; a precipitation endotherm commences just above the precipitation range. The curves are shifted vertically to avoid overlap.

this loss of early-time data have been discussed previously [31], as have methods to account for possible baseline drift [32]. As for DSC scans, isothermal dQ/dt curves can be either endothermic or exothermic. The total energy, ΔQ, absorbed or released during the isothermal process is determined by integrating dQ/dt vs. t.

3. Methods of analysis and results

Although the analytical methods have been described previously for air-cooled alloy 339 [33], it is appropriate to review their salient features since, in the case of SOL alloy 2124, they are applied to a wider range of thermal events.

3.1. Scanning experiments – the Kissinger analysis

The Kissinger method [24,28] for deriving activation energies from temperature-scanned experiments is based on the fact that the temperature, T_p, of a peak extremum depends on the scan rate, S=dT/dt, of the experiment. For slow scan rates, peaks occur at lower temperatures than for fast scan rates, as seen in Fig. 1, where dQ/dt is plotted vs. T for SOL 2124 at scan rates ranging from 1.2 to 80°C/min. The peak intensity is proportional to S and, thus, decreases as the scan rate is reduced. Yet another effect of scan rate is seen in Fig. 1. For the five lowest values of S it is clear that, in addition to a single low temperature peak due to GP zone formation [19], there are two precipitation peaks at higher T. At the two highest scan rates (S=40 and 80°C/min), the GP exotherm is still isolated, but the precipitation peaks have coalesced. This peak coalescence complicates the determination of T_p values for high scan rates, and reinforces our prior conclusion [33] that the Kissinger analysis yields reliable kinetics results only for sufficiently slow scan rates, in accordance with the conclusions of Badini et al. [22] (see also below). In addition to GP and precipitation peaks, Fig. 1 exhibits the above-mentioned GP zone and precipitate dissolution endotherms which, although they interfere with the evaluation of ΔQ, do not greatly affect the determination of T_p values.

Under appropriate conditions, the Kissinger equation can be applied to each of the peaks in turn. As modified by Mittemeijer et al. [28], it is given by:

$$\ln(T_p^2/S) = E_{act}/(RT_p) + \ln(E_{act}/Rk_0). \quad (1)$$

Here E_{act} is an effective activation energy, R the gas constant, and k_0 the pre-exponential factor in the Arrhenius equation for the rate constant k:

$$k = k_0 \exp(-E_{act}/RT) \quad [or\ \tau_{Kiss} \equiv 1/k = \tau_0 \exp(E_{act}/RT)]. \quad (2)$$

Applicability of the Kissinger analysis to GP and precipitate formation peaks requires that the fraction of species transformed, X_p, should be independent of scan rate [22]. The reciprocal of the Kissinger rate constant given by Eq. (2) should be regarded as an average time constant for a given DSC peak since it lumps together any and all contributing precipitation mechanisms. Substitution of Eq. (2) into Eq. (1) yields a rather simple expression for k_p, the value of k at temperature T_p:

$$k_p = (E_{act}/R) \times (S/T_p^2), \quad (3)$$

In Eqs. (1) and (3), S is expressed in K/s (or °C/s) so that k will have units of s^{-1}.

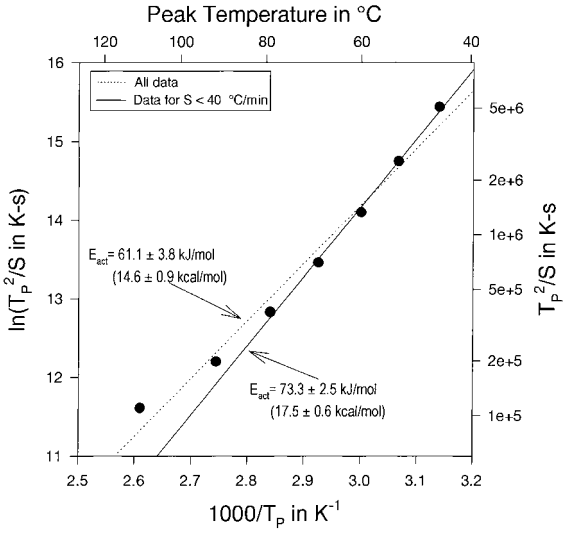

Fig. 2. Kissinger plot for the exothermic peak due to GP zone formation in SOL alloy 2124. The lines are fits of Eq. (1) to the data (see text).

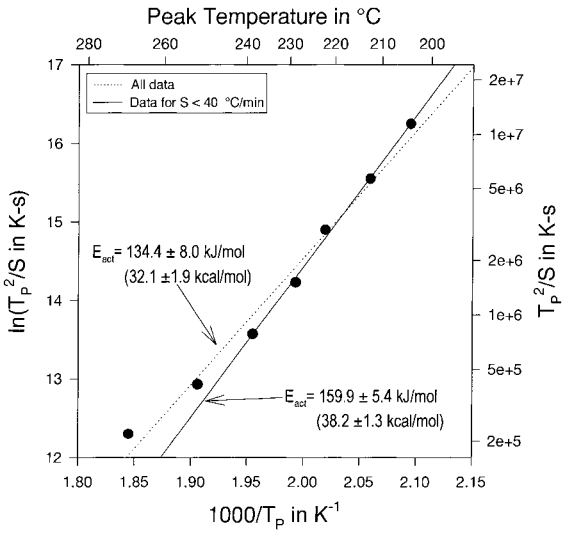

Fig. 3. Kissinger plot for the endothermic peak due to GP zone dissolution in SOL alloy 2124. The lines are fits of Eq. (1) to the data (see text).

3.1.1. Application to GP zone formation and dissolution

The Kissinger analysis of the GP zone formation peak of SOL 2124 is illustrated in Fig. 2, where we plot two linear fits of Eq. (1), using values of T_p derived from the DSC curves of Fig. 1. The dotted line fit includes data for all scan rates; the solid line fit excludes T_p values for S=40 and 80°C/min. As was the case for precipitation in ACO alloy 339 [33], exclusion of data for too-fast scans decreases adverse instrumental lag time effects. The value of S is sufficiently slow if we scan through a DSC peak in a time longer than τ_{lag}. Expressed as an inequality, this requirement becomes [33]

$$(1/\Delta T)(dT/dt) = S/\Delta T < 1/\tau_{lag}. \quad (4)$$

For the GP zone formation peak of Fig. 1, $\Delta T \approx 40$°C. Since the instrumental lag time is one minute or less, only scan rates <40°C/min should be used for the Kissinger analysis. Thus, the solid line in Fig. 2 is based only upon T_p values for scan rates from 1.2 to 20°C/min. We confirmed the applicability of the Kissinger analysis of the GP peak in this scan-rate range by integration (as described in Ref. [7]), obtaining a nearly constant value for X_p (0.40±0.015).

It is possible to estimate GP zone dissolution kinetics from DSC [1], but not from DIC. Fig. 3 shows two Kissinger plots for the GP dissolution endotherms of Fig. 1. As in the case for GP zone formation, only data for the five slowest scan rates should be used. The derived activation energy (~160 kJ/mol) is somewhat higher than previous results for other aluminum alloys (~126 kJ/mol) [1,6], but lower than the value for dissolution of GP zone/dislocation complexes (~210 kJ/mol) [6]. Values of Kissinger parameters for GP zone formation and dissolution are given in the Appendix (sections A and B of Table A.1).

3.1.2. Application to precipitation exotherms

Figs. 4 and 5 show Kissinger plots for the first and second precipitation peaks of Fig. 1. Since, as mentioned above, the two peaks coalesce for S>20°C/min, determining peak positions for the two highest scan rates was less precise than for the five slowest rates. (For S=40°C/min, T_p values were estimated from the positions of the 'shoulders' in the scan of Fig. 1. For the 80°C/min scan, the position of the peak extremum (341.0°C) was used as the value of T_p for both the precipitation peaks (i.e. in both Figs. 4 and 5). In Fig. 4, it appears that a good fit is attainable only if the data for the two fastest scan rates are excluded. In Fig. 5, a good fit is achieved whether or not all the points are included. Since the second precipitation peak seems broader than the first peak, it may be less

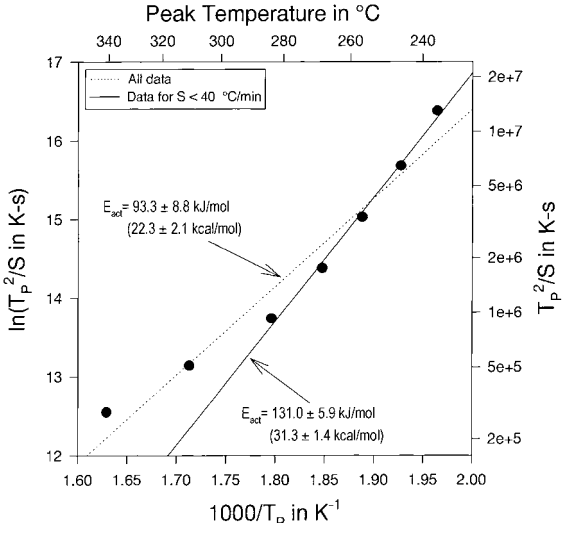

Fig. 4. Kissinger plot for the first precipitation peak in SOL alloy 2124. The lines are fits of Eq. (1) to the data (see text).

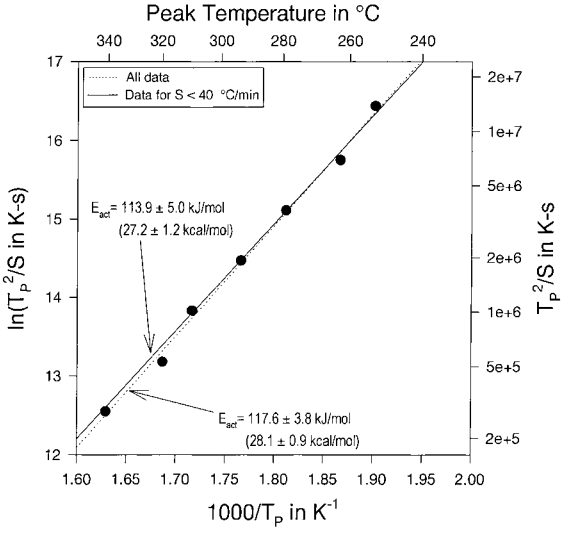

Fig. 5. Kissinger plot for the second precipitation peak in SOL alloy 2124. In contrast to the behavior of Figs. 2–4, a single regression fit of Eq. (1) passes through all the data.

susceptible to instrumental lag time effects (see Eq. (4)). By deconvoluting the precipitation doublet for S<20°C/min, we found that the X_p values of the two peaks are fairly constant, thus validating the use of the Kissinger analysis in this regime as well that for GP zone formation. (It should be noted that this result

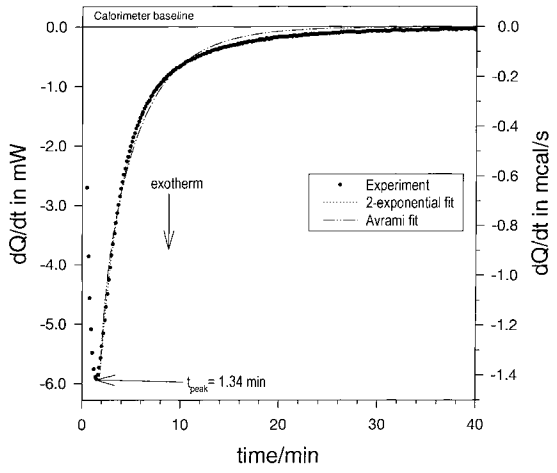

Fig. 6. Isothermal calorimetry curve of dQ/dt vs. time for GP zone formation in a sample of SOL alloy 2124 at 60°C. Techniques discussed in the text were used to determine several time constant(s) from the curve. Arrhenius plots of the various time constants yield effective activation energies for the GP zone formation process (see Figs. 7–10).

is consistent with the Badini condition [22] that, in order to apply Kissinger-type analyses to overlapping peaks, the shape of DSC scans should be independent of scan rate.) Values of Kissinger parameters for the precipitation peaks are given in the Appendix (sections C and D of Table A.1).

3.2. *Isothermal experiments – GP zone formation ($T \leq 100$°C)*

A typical isothermal calorimetry curve for GP zone formation in SOL 2124 is shown in Fig. 6, where dQ/dt is plotted vs. time at 60°C. From such isotherms, it is possible to derive several time constants. Some of these time constants have been discussed elsewhere [31–33]. Therefore, we shall review them only briefly, illustrating their determination using Fig. 6.

3.2.1. *Delay time derived from peak of dQ/dt*

The simplest time constant to determine is t_{peak}, the delay time before dQ/dt reaches its peak value. Although t_{peak} values for precipitation in air-cooled samples are usually small [33], delay times for GP zone formation and precipitation in solutionized/water-quenched samples can be sizable. In Fig. 6, t_{peak} is 1.34 min. It is reasonable to assume that t_{peak}

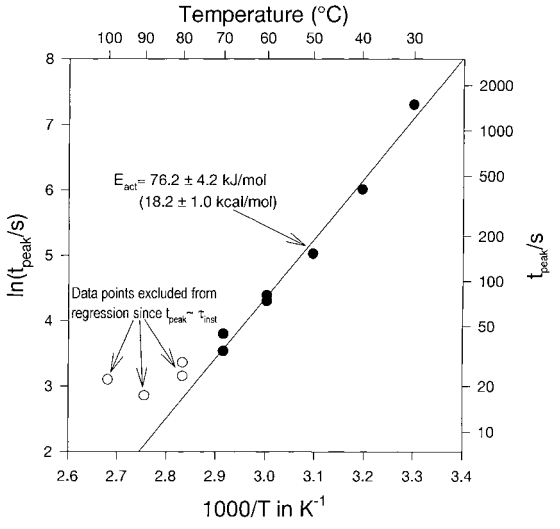

Fig. 7. Arrhenius plot of t_{peak} for GP zone formation in SOL alloy 2124. The line is a best regression fit to the data, excluding four data points at temperatures above 70°C, for which t_{peak} is comparable to τ_{lag}.

obeys an Arrhenius-like equation:

$$\ln t_{peak} = \ln t_0 + E_{act}/RT, \quad (5)$$

since GP zone nuclei must form, and dissolved species must diffuse to them before dQ/dt can reach its maximum rate. Both processes should obey the Arrhenius relation.

Fig. 7 shows the corresponding Arrhenius plot. A good fit of Eq. (5) is obtained if the data points for the four highest temperatures are excluded. The exclusion of these points is appropriate since the values of t_{peak} are comparable to the instrumental lag time ($\tau_{lag} \approx 1$ min).

3.2.2. *Time constants derived from fits to decaying portion of dQ/dt*

Other time constants are obtained from fits of analytical expressions to the decaying portion of dQ/dt [33]. One such analysis is the 2-exponential fit, from which two time constants (τ_1 and τ_2) are determined. In addition, two 'average' time constants can be defined. The first of these, the rate-averaged time constant (τ_{rate}), is derived from τ_1 and τ_2 [33]; the second, τ_{Avrami}, is determined by fitting Avrami-type curves directly to dQ/dt [32]. Activation energies are derived from Arrhenius plots of these four time constants.

One of the purposes of the present study is to establish criteria which will enable us to determine when the 2-exponential model is appropriate and when an average time constant is best for analysis of DIC experiments. We shall argue that the 2-exponential analysis is particularly relevant when precipitation involves two important processes (indicated by the presence of two separate DSC peaks or more than one clearly distinct decay process in DIC curves). On the other hand, when a single mechanism is dominant (as indicated by the existence of a single peak in DSC scans and nearly exponential decay behavior in DIC runs), precipitation kinetics can best be described by an average time constant. In this latter case, τ_{rate} is the isothermal average time constant which gives best agreement with the DSC time constant, $1/k$.

3.2.2.1. 2-exponential analysis. This analysis can be justified by assuming that, after the initial delay time, two species precipitate to evolve heat at a rate given by [33]

$$dQ/dt = -\alpha_1 \exp(-t/\tau_1) - \alpha_2 \exp(-t/\tau_2). \quad (6)$$

Here, each of the exponential terms represents the precipitation kinetics of a single species, with $\tau_1 < \tau_2$. (A mathematical interpretation of Eq. (6) is that it merely represents the first two terms in a series approximation to the data.) The fit of the 2-exponential expression to the experimental curve in Fig. 6 is extremely good, essentially coinciding with the data. In fact, fits are good for all temperatures >30°C. Generally, α_1 is significantly larger than α_2, suggesting that the fast process is dominant. However, a more suitable test for the relative importance of the fast and slow processes is provided by comparing the contribution each makes to ΔQ, the heat release during GP zone formation or precipitation (see below).

The temperature dependences of the fast (τ_1) and slow (τ_2) processes are usually well described by the Arrhenius equation [33]. This is illustrated in Fig. 8 for GP zone formation in SOL 2124. The activation energy for the dominant term (τ_1) is almost identical to that found from t_{peak} (Fig. 7).

3.2.2.2. Rate-averaged τ derived from 2-exponential analysis. As argued above, average time constants are meaningful when two processes (one of which is

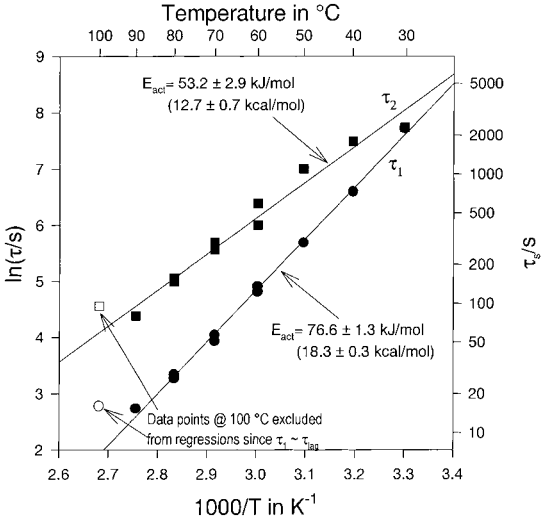

Fig. 8. Arrhenius plots of τ_1 and τ_2 from 2-exponential fit for GP zone formation in SOL 2124. Lines are best fits to the data, neglecting results for 100°C for which τ_1 is comparable to τ_{lag}.

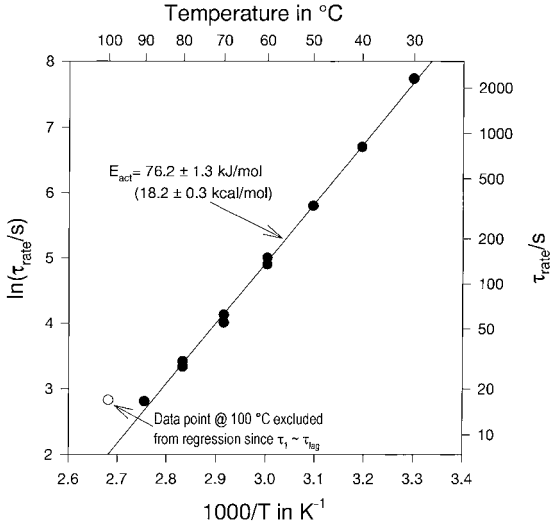

Fig. 9. Arrhenius plot of τ_{rate} derived from 2-exponential fit parameters of Fig. 8 and Table 6 for GP zone formation in SOL 2124. Line is best fit to the data, neglecting value for 100°C for which τ_1 is comparable to τ_{lag}.

dominant) contribute simultaneously to a single DSC precipitation peak. This seems to be the case for GP zone formation, which is characterized by a single DSC peak (Fig. 1) and nearly exponential decay of the DIC curve (Fig. 6). Thus, it is relevant to compare average time constants from isothermal experiments with those from scanning calorimetry. The rate-averaged time constant τ_{rate}, is given by [33]:

$$\tau_{rate} = \tau_1\tau_2(\alpha_1 + \alpha_2)/(\alpha_1\tau_2 + \alpha_2\tau_1). \quad (7)$$

Fig. 9 shows the Arrhenius plot of τ_{rate} for GP zone formation in SOL alloy 2124. Although E_{act} for τ_{rate} is equal to that for τ_1 (indicating that the fast process is dominant), the rate-averaged time constant values are ~10% slower than those for τ_1.

3.2.2.3. Avrami time constant. Average kinetics of phase transformations, including diffusion-controlled precipitation, can often be described by the Avrami equation [35]

$$X(t) = 1 - \exp\left[-(t/\tau_{Avrami})^n\right], \quad (8)$$

where $X(t)$ is the fraction of material transformed or precipitated, t the time, τ_{Avrami} the time constant, and n a constant. Avrami time constants can be derived directly from isothermal data by fitting the decaying portion of the dQ/dt curves to the equation [32]. The fact that n is not truly constant has been pointed out elsewhere [32,36].

$$dQ/dt = -C(n(t - \Delta t)^{n-1}/\tau^n_{Avrami}) \exp\left(-((t - \Delta t)/\tau_{Avrami})^n\right) \quad (9)$$

where C is a constant, and Δt a time shift. In Fig. 6, we show a best fit of Eq. (9) to dQ/dt, in addition to the 2-exponential fit (Eq. (6)). The former does not represent the data as well as the latter for any temperature >30°C (see Table A.1). Thus, E_{act} from the Arrhenius plot of τ_{Avrami} (Fig. 10) is ~15% lower than values determined by the other isothermal analyses. As was the case for precipitation in air-cooled alloy 339 [33], τ_{Avrami} is not a reliable average time constant for GP zone formation in alloy 2124.

3.2.3. Heat release, ΔQ, during GP zone formation

The most accurate values of ΔQ are determined by integrating DIC dQ/dt curves [33] (e.g., for Fig. 6, ΔQ=−14.1 J/g). Fig. 11 plots ΔQ vs. T for GP zone formation in SOL 2124. At high T, ΔQ decreases due to loss of early-time data as the time constant for GP zone formation becomes small (comparable to τ_{lag}). We can resolve ΔQ into two contributions, ΔQ_1 and

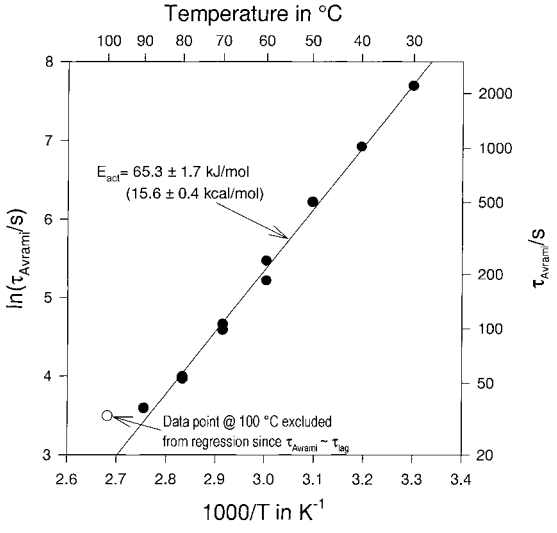

Fig. 10. Arrhenius plot of τ_{Avrami} for GP zone formation in SOL 2124. Line is best fit to the data, neglecting value for 100°C for which τ_{Avrami} is comparable to τ_{lag}.

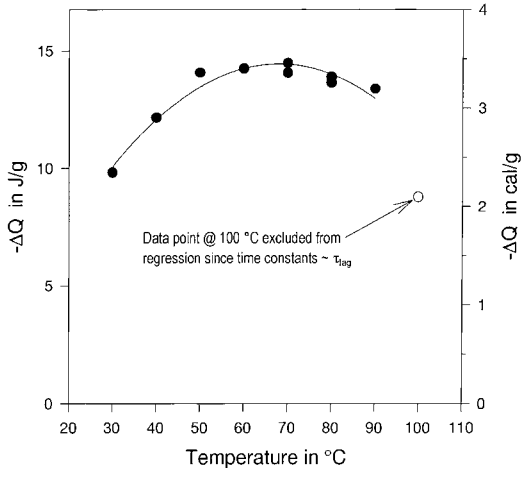

Fig. 11. Heat released, ΔQ, during GP zone formation in SOL 2124 at various temperatures. ΔQ values were determined by integrating DIC curves of dQ/dt vs. time like that of Fig. 6. The curve is quadratic regression fit to data, excluding points at 100°C for which time constants are comparable to τ_{lag}.

ΔQ_2, from the fast and slow processes by an approximate equation which takes into account the initial rise of dQ/dt to its extremum at t_{peak}:

$$\Delta Q_i = (\alpha_i \tau_i / \mathrm{m})(t_{\text{peak}}/2 + \tau_i)\exp(-t_{\text{peak}}/\tau_i). \quad (10)$$

Here, i=1 or 2, α_i and τ_i are 2-exponential fit parameters, and 'm' the sample mass. According to Eq. (10), the fast (τ_1) process contributes ca. 60% of the total heat release at temperatures from 40° to 100°C, indicating that it does, indeed, dominate GP zone formation. In the Appendix (Part A of Table A.2) are summarized ΔQ values, as well as time constants and fitting parameters of the 2-exponential and Avrami models for GP zone formation.

3.3. Isothermal experiments – precipitation (T>210°C)

The analytical methods of Section 3.2 will now be applied to precipitation in SOL 2124. It should be emphasized that several factors, including competition between GP zone formation and dissolution (which varies rapidly with temperature), make it essentially impossible to obtain meaningful isothermal time constants in the temperature range from 100° to 210°C.

Fig. 12 shows a typical isothermal calorimetry curve of dQ/dt vs. time for precipitation in SOL 2124 at 240°C. The value of t_{peak} is indicated in the figure; in addition, regressions of both the 2-exponential and Avrami models are plotted. Again, the former

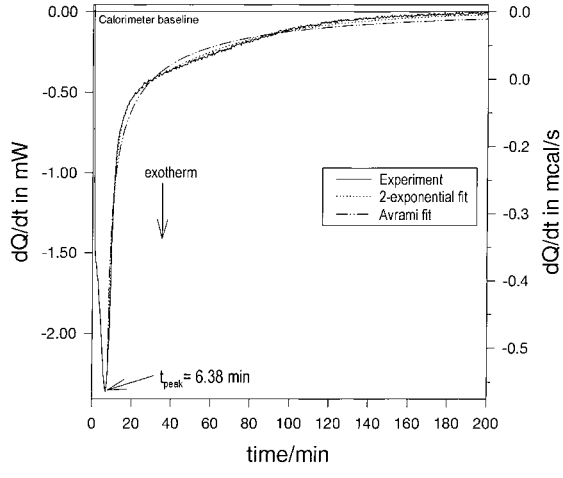

Fig. 12. Isothermal calorimetry curve of dQ/dt vs. time for precipitation in SOL alloy 2124 at 240°C. Techniques discussed in the text were used to determine time constant(s) for precipitation in the alloy. From Arrhenius plots of the time constants, effective activation energies for the precipitation process were determined (see Figs. 13 and 14).

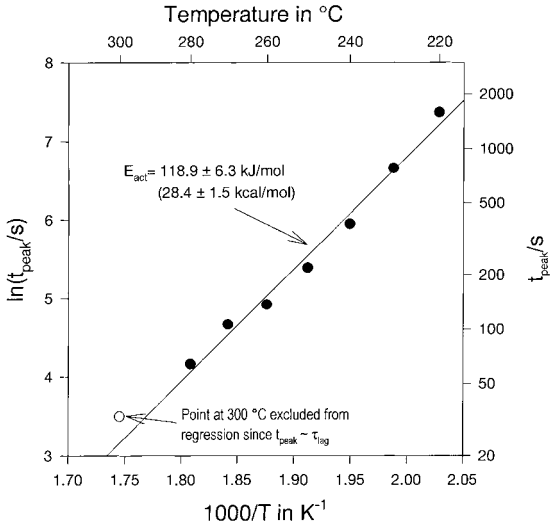

Fig. 13. Arrhenius plot of t_{peak} for precipitation in SOL alloy 2124. The line is a best regression fit to the data, excluding the data point at 300°C, for which t_{peak} is comparable to τ_{lag}.

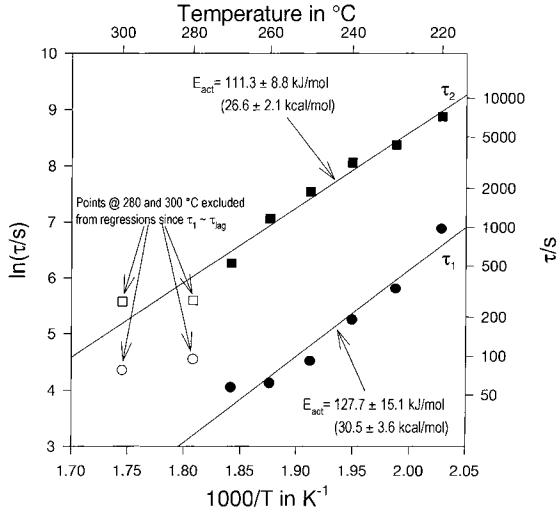

Fig. 14. Arrhenius plots of τ_1 and τ_2 from 2-exponential fit for precipitation in SOL 2124. Lines are best fits to the data, neglecting results for 280° and 300°C for which τ_1 is comparable to τ_{lag}.

fits the experimental curve much better than does the latter for all temperatures >210°C. The existence of both, fast and slow contributions to the precipitation process is quite apparent in Fig. 12, suggesting that they may be associated, respectively, with the first and second precipitation peaks in the DSC scans of Fig. 1. This point will be examined in greater detail in Section 4.

3.3.1. Delay time derived from peak of dQ/dt

Fig. 13 is an Arrhenius plot of t_{peak}, derived from curves like that of Fig. 12. To fit Eq. (5) to the data, we exclude the point for 300°C, since it is comparable to τ_{lag}. The derived activation energy is considerably larger than that for GP zone formation (Fig. 7).

3.3.2. Time constants derived from fits to decaying portion of dQ/dt

Fig. 14 shows Arrhenius plots for the time constants τ_1 and τ_2 from the 2-exponential analysis. For all but the questionable data points at the two highest temperatures, τ_2 is at least an order of magnitude greater than τ_1, indicating the existence of two distinct precipitation processes. (By way of contrast, τ_1 and τ_2 in Fig. 8 are, for the most part, closer in magnitude, suggesting that GP zone formation is not readily separable into two mechanisms.) In carrying out the regression fits to the data of Fig. 14, the points at the two highest temperatures are questionable since $\tau_1 \sim \tau_{lag}$, and were therefore excluded. The temperature range of the valid data points is rather limited, so that there is a sizable uncertainty in E_{act}. The existence of two precipitation processes in SOL 2124 (Figs. 12 and 14), indicates that analysis by a single average time constant such as τ_{rate} or τ_{Avrami} is inappropriate in this regime.

3.3.3. Heat release, ΔQ

Fig. 15 plots ΔQ vs. temperature for the entire experimental temperature range (30–300°C). The maximum heat released during precipitation (~26.8 J/g at ~270°C) is almost twice that for GP formation (~14.7 J/g at ~70°C). Resolution of ΔQ into contributions from the fast and slow precipitation processes (using Eq. (10)) shows that the slow process is of major importance, contributing 60–70% of the total heat release. The relative magnitudes of ΔQ_1 and ΔQ_2 provide an additional criterion for choosing the appropriate isothermal analysis method (see Section 5.1). Values of ΔQ, time constants, and 2-exponential α-values for precipitation are given in the Appendix (section B of A.2).

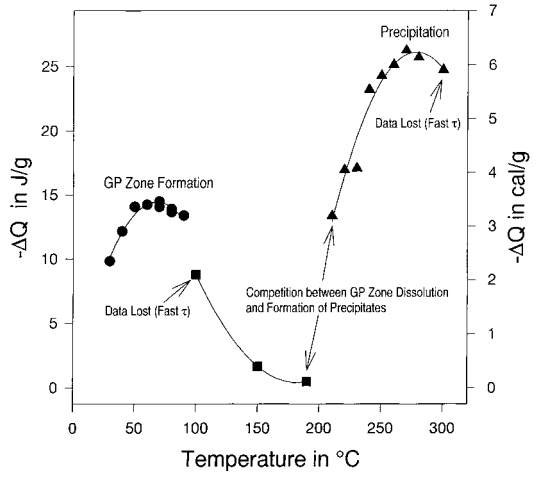

Fig. 15. Heat released, ΔQ, during GP zone formation and precipitation in SOL 2124 at various temperatures. ΔQ values were determined from isothermal calorimetry curves of dQ/dt vs. time, such as that of Figs. 6 and 12. Curves are quadratic regression fits to data.

4. Discussion

4.1. Activation energies

Table 1 summarizes values of activation energies for SOL alloy 2124 determined by both scanning and isothermal calorimetry. Let us briefly review the results.

4.1.1. GP zone formation

We have suggested in the foregoing that, under certain conditions, it is appropriate to compare the DSC activation energy to that from the rate-averaged DIC time constant. Those conditions include a single DSC peak and nearly exponential decay of the DIC curves, as observed for GP zone formation in alloy 2124. The agreement of the two values of E_{act} is good (73.3 vs. 76.2 kJ/mol). The fact that E_{act} from t_{peak} is identical to the value from τ_{rate} indicates that the same mechanisms control both the position of the peak extremum and the decay rate of dQ/dt. At low temperatures, nucleation and diffusion of precipitate species are apparently so slow that GP zones cannot form. Thus, when the temperature is raised to the range for GP zone formation, both processes may contribute to the activation barrier.

4.1.2. GP zone dissolution

As discussed above, it was possible to determine the kinetics of GP zone dissolution only by scanning calorimetry. The activation energy, 160 kJ/mol, from DSC (Fig. 3) is higher than the values reported for GP zone formation in Al/6.2%Cu (126 kJ/mol) [1] and in Al/1.53%Cu/0.79%Mg (124 kJ/mol) [6]. However, E_{act} for dissolution of GP zone/dislocation complexes in the ternary alloy (~210 kJ/mol) [6] is considerably greater than our GP zone result. The possibility cannot be ruled out that the GP zone dissolution peak for alloy 2124 also involves such complexes.

4.1.3. Precipitation

Precipitation in SOL 2124 seems to be occurring via two distinct processes. We suggest that the fast (τ_1) and slow (τ_2) processes from DIC (2-exponential analysis) are associated with the first and second DSC precipitation exotherms, respectively. A comparison of the activation energies indicates that this association is reasonable: The isothermal values of E_{act} from τ_1 and τ_2 (128 and 111 kJ/mol) are equal (within experimental error) to the scanning values for the two peaks (131 and 114 kJ/mol).

Table 1
Activation Energies for SOL Alloy 2124 (present work) (Activation energies [a] in kJ/mol)

Process	DSC[b]	Differential isothermal calorimetry			
	Kissinger	from t_{peak}	from τ_1	from τ_2	from τ_{rate}
GP zone formation	73.3±2.5	76.2±4.2	76.6±1.3	53.2±2.9	76.2±1.3*
GP zone dissolution	159.9±5.4	—	—	—	—
First precipitation process	131.0±5.9	118.9±6.3	127.7±15.1	—	—
Second precipitation process	113.9±5.0	—	—	111.3±8.8	—

[a] E_{act} values from τ_{Avrami} differ from other values (see text). Also τ_{rate} is useful only for analysis of a single process like GP zone.
[b] Differential scanning calorimetry.

Mishra [37] has carried out transmission electron microscope (TEM) studies of samples held at four temperatures ranging from 190° to 300°C. At 190°C, only S' ($CuMgAl_2$) was observed. At 230°C, he detected a small amount of θ' ($CuAl_2$) which increased with further temperature increases. At 300°C, the two phases were almost equal in concentration. Thus, it appears that the precipitate associated with the first precipitation peak is S' and that, for the second peak, it is θ'. As will be seen below, this result seemingly conflicts with other conclusions in the literature.

4.2. Comparison of scanning and isothermal time constants

4.2.1. GP zone formation

In Fig. 16 are Arrhenius plots of average time constants from both DSC and DIC, and also of τ_1 from DIC. The plot for the best isothermal average, τ_{rate}, agrees well with that for $1/k$ derived from the Kissinger analysis of the DSC peaks. (Similar close agreement between $1/k$ and τ_{rate} was noted for precipitation in air-cooled alloy 339 [33]). It is more suitable to compare the DSC time constant to τ_{rate} than to τ_1 (both of which have comparable values of E_{act})

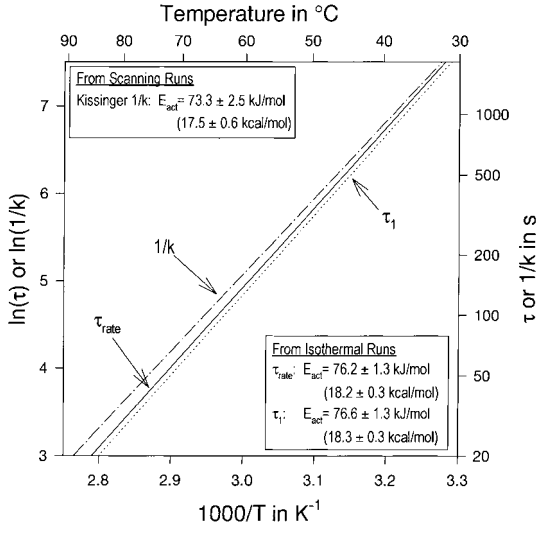

Fig. 16. Arrhenius plots of time constants for GP zone formation in SOL 2124: Regression fits are shown for average time constants from DSC ($1/k$) and from DIC (τ_{rate}), as well as for τ_1, the fast time constant from the two exponential fit. Although τ_1 appears comparable to τ_{rate}, it is actually about 10% smaller.

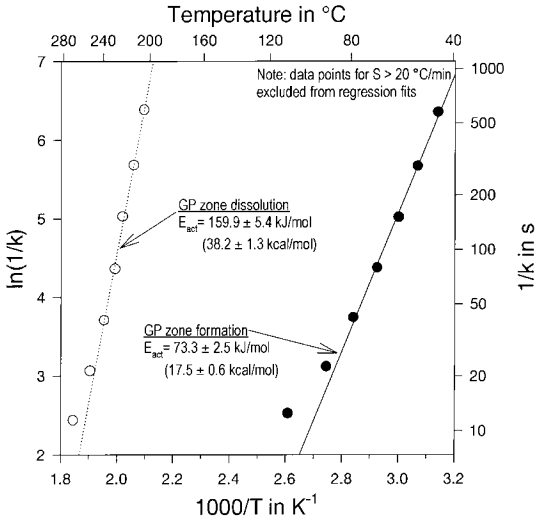

Fig. 17. Arrhenius plots of regression fits to DSC time constants ($1/k$) for GP zone formation and dissolution in SOL 2124.

because the DSC/Kissinger $1/k$ values for GP zone formation are implicitly *average* time constants.

4.2.2. GP zone dissolution

Fig. 17 plots Kissinger time constants ($1/k$) for both GP zone formation and dissolution. The dissolution time constant varies rapidly with temperature: within a few °C, it decreases by an order of magnitude. This temperature sensitivity, the rapidity of the process, and the competition of other processes (GP zone formation and precipitation) all make isothermal studies of GP zone dissolution difficult, if not impossible.

4.2.3. Precipitation

Since precipitation in SOL alloy 2124 seems to involve both a fast and a very slow process, it is relevant to compare time constants $1/k_1$ and $1/k_2$ from Kissinger analyses of the first and second DSC precipitation peaks to values of τ_1 and τ_2 from the 2-exponential analysis of DIC curves. Fig. 18 gives Arrhenius plots of both $1/k_1$ and $1/k_2$, and τ_1 and τ_2. Although the agreement for the scanning and isothermal values for precipitation is not as good as it was for GP zone formation, it is satisfying that these time constants, derived from dissimilar analyses of different techniques, are at least comparable in magnitude. The discrepancies may be due, in part, to the overlapping of the DSC peaks, resulting in larger experi-

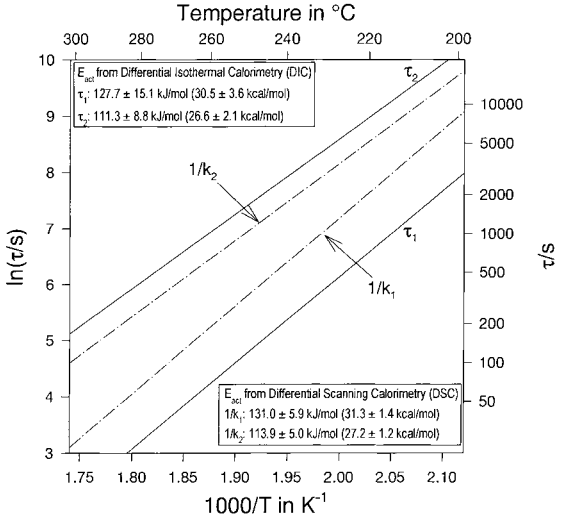

Fig. 18. Comparison of Arrhenius plots of regression fits to fast and slow time constants from DSC ($1/k_1$ and $1/k_2$) and DIC (τ_1 and τ_2) for precipitation in SOL 2124.

mental errors of E_{act} for precipitation. (Reducing E_{act} for $1/k_1$ from 131 to 128 kJ/mol, the value for τ_1, decreases $1/k_1$ by a factor of 2, bringing it into approximate agreement with τ_1.) Of possibly greater significance than the time constant differences is the agreement of the E_{act} values from the two methods.

4.3. Comparisons with literature

4.3.1. Prior DSC studies of solution-treated alloy 2124

Papazian [5] conducted a DSC study of solution-treated alloy 2124 (composition not stated). He reported a GP formation peak but only a *single* precipitation exotherm (at 10°C/min), which he ascribed to the formation of a metastable S' phase (Al_2CuMg). Thomas and King [21] obtained similar results for alloy 2124 (again composition not given) and arrived at the same conclusions. (Unfortunately, neither author reports activation energies.) Table 2 shows that our T_p values for the GP zone formation peak and for the *first* precipitation peak agree well with theirs.

4.3.2. DSC studies of related alloys

4.3.2.1. Alloy 2024. Badini et al. [22] carried out an in-depth DSC study of SOL alloy 2024 (4.25% Cu/1.3% Mg). Since the composition and solution treatment of their alloy are comparable to those of our alloy 2124, it is useful to compare their results to ours. They discussed two possible precipitation schemes: (1) GP zones$\rightarrow\theta''\rightarrow\theta'\rightarrow\theta$ ($CuAl_2$) and (2) GP zones $\rightarrow S'\rightarrow S$ ($CuMgAl_2$). Depending on the Cu content and the Cu : Mg ratio, these processes can occur separately or simultaneously. For scan rates <30°C/min, they observed a GP zone formation peak and *two* precipitation exotherms; at 50°C/min, the two precipitation peaks coalesce. The temperatures of both 2024 precipitation peaks are close to those for our SOL 2124 (see Table 3). Badini et al. associated the peaks with overlapping θ'' and S' formations. From an Ozawa [25] analysis of the peak temperatures, they derived activation energies of 117–130 kJ/mol for the first peak and 130 kJ/mol for the second. We re-analyzed their T_p data using the Kissinger method to obtain E_{act}=126±7 and 135±3 kJ/mol, respectively. (Our analysis of the first peak excluded the point for 30°C/min since the peak appears as little more than a shoulder in the DSC scan.)

The Kissinger time constants for SOL 2124 and 2024 are compared in Fig. 19. The time constants and activation energies for the first peak are nearly equal

Table 2
Scanning calorimetry data for SOL 2124 (powder metallurgy samples, scan rate=10°C/min)

Reference	Solution treatment[a]	Peak temperature (°C)		
		GP zone formation	Precipitation	
Papazian [5] [b]	520°C/1 h, WQ,−196°C	67	263	—
Thomas and King [21] [b]	505°C/2 h, WQ,?	67.3	265	—
Present work [c]	495°C/1 h, WQ,−74°C	68.6	268	293

[a] Solution treatment temperature/duration; WQ, water quench; last entry, storage temperature after quench.
[b] Sample composition not stated.
[c] Sample composition given in Table 4.

Table 3
Scanning calorimetry data for precipitation in SOL 2024 and 2124

Scan Rate (°C/min)	T_p for first peak (°C)		T_p for second peak (°C)	
	alloy 2024 [a]	alloy 2124 [b]	alloy 2024 [a]	alloy 2124
1.2		235.8		252.5
2.0	245		265	
2.5		245.7		262.5
5.0	258	256.4	279	278.8
10.0	271	268.0	292	293.0
20.0	286	283.5	306	309.4
30.0	306		314	
40.0		310.6		319.6
50.0	325		325	
80.0		340.6		340.6

[a] Badini et al. [22] (solution treatment: 495°C/2 h, brine quench, stored in liquid N_2). T_p for GP zone formation not given.
[b] Present work.

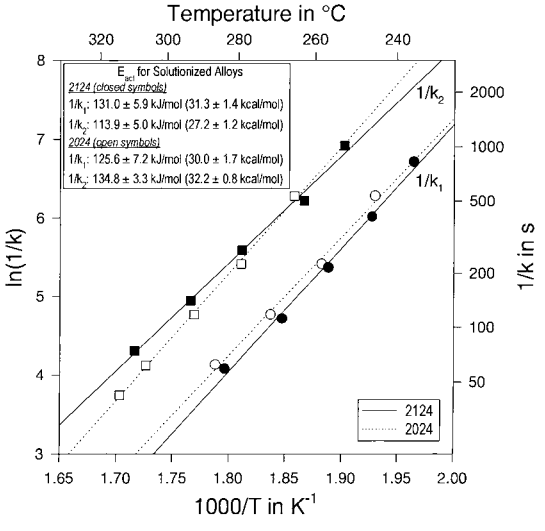

Fig. 19. Comparison of Arrhenius plots of $1/k_1$ and $1/k_2$ values derived from first and second DSC precipitation peaks of solutionized 2124 and 2024. The points for 2024 were calculated from the data of Badini et al. Lines are best regression fits.

for the two alloys, indicating that the same mechanism may be involved in each. The activation energy for the second 2024 peak is almost 20% higher than that of 2124, so that we cannot conclude that the same precipitation mechanisms occur in both alloys. Badini et al. compared their work with prior studies of similar alloys and proposed that the first peak was due to θ'' and the second to $\theta'+S'$. However, as discussed above, the TEM results of Mishra [37] indicate that the S' phase forms at a lower temperature than the θ' phase. He points out that this sequence is consistent with the facts that S' forms by heterogeneous nucleation, while θ' nucleates homogeneously.

4.3.2.2. Alloy 2014. Dutta et al. [19] used scanning and rather limited isothermal calorimetry to study solutionized alloy 2014 (4.57% Cu/0.42% Mg/0.66% Si, plus other elements). Only three DSC scan rates (5, 10, and 20°C/min) were used; for the intermediate scan rate they observed a GP zone formation peak at ~77°C and two precipitation peaks at ~234 and ~285°C. The first of these they ascribed to λ' ($Al_5Cu_2Mg_8Si_5$) formation and the second to θ' formation. From non-Kissinger analyses, they derived activation energies of 70, 80 and 82 kJ/mol for the three peaks. Since they did not cite T_p values for all their scan rates, we could not re-analyze their data to derive Kissinger activation energies. The GP zone formation activation energy for alloy 2014 is comparable to that for alloy 2124. However, the E_{act} values for precipitation in the former are considerably smaller than those for both 2124 and 2024, which is not surprising since the Mg and Si contents of the two alloys are quite different. Activation energies and precipitate information (where known) for all three alloys are summarized in Table 4.

5. Summary

Several useful findings resulted from this work. These include aspects relevant to the measurement and analysis techniques as well as to the material studied.

5.1. Measurement and analysis techniques

The scan-rate restriction ($S/\Delta T<1/\tau_{lag}$) for Kissinger analysis of DSC experiments, previously validated only for air-cooled alloy 339 [33], has been found to apply also to the calorimetrically more complex case of solution-treated alloy 2124.

Our studies of this alloy have led to criteria for selecting the proper DIC time constants to compare

Table 4
DSC results for SOL 2124, 2024, and 2014 [f]

Alloy	Cu	Mg	Si	GP zone	1st precipitation peak		2nd precipitation peak		Ref.
				E_{act} [a]	E_{act} [a]	Ppt.	E_{act} [a]	Ppt.	
2124	4.5	1.6	0.1	73.3±2.5	131.1±5.9	S' [b]	113.9±5.0	θ' [b]	Present work
2024	4.25	1.3	—		117–130 [c]	θ'	130[c]	$\theta'+S'$	Badini et al. [22]
2024	4.25	1.3	—		125.6±7.2 [d]	θ'	134.8±3.3[d]	$\theta'+S'$	Badini et al. [22]
2014	4.57	0.42	0.66	69.5 [e]	80.4 [e]	λ'	82.1[e]	θ'	Dutta et al. [19]

[a] E_{act} in kJ/mol.
[b] TEM results of Mishra.
[c] Badini analysis.
[d] From our Kissinger analysis of Badini data.
[e] From non-Kissinger analysis in original reference.
[f] Solution treatment for 2014: 520°C/1.5 h; ice water quench, followed immediately by calorimetry run.

with Kissinger time constants from analyses of DSC curves. When one mechanism dominates a precipitation process, a single average time constant (τ_{rate}) should be used. This situation is indicated by three factors:

1. The process is associated with a single isolated exothermic peak in DSC scans.
2. Isothermal dQ/dt curves are characterized by nearly exponential decays. That is, no more than one decay process is clearly distinguishable in the DIC curves (generally, τ_1 and τ_2 differ by less than an order of magnitude and $\alpha_1 \gg \alpha_2$).
3. ΔQ_1, the exothermic heat contributed to ΔQ by the fast precipitation process, is greater than the amount ΔQ_2 due to the slow process.

When precipitation clearly involves two processes, the 2-exponential time constants should be compared individually with the Kissinger results. In this case the three indicators are:

1. Two peaks (perhaps partially overlapping) are present in the DSC scans.
2. Two distinct decay processes are evident in the DIC curves (with $\tau_2 \geq 10\tau_1$).
3. $\Delta Q_2 \geq \Delta Q_1$.

GP zone formation in SOL alloy 2124 fulfils the first set of criteria so that the use of the rate-averaged time constant, τ_{rate}, is appropriate. This conclusion is in accordance with that reached for precipitation in ACO alloy 339 [33]. In both cases, there is good agreement between plots of τ_{rate} and Kissinger $1/k$ values. On the other hand, as for alloy 339, τ_{Avrami} differs from $1/k$ in both its magnitude and its activation energy. Thus, τ_{Avrami} is again not a suitable average time constant.

Precipitation in SOL 2124 satisfies the second set of criteria. Thus, τ_1 and τ_2 are appropriate time constants for the two processes associated with the first and second DSC precipitation peaks. The DSC activation energies for each peak agree quite well with the corresponding values from DIC. However, the scanning/Kissinger time constants ($1/k_1$ and $1/k_2$) differ somewhat from the isothermal τ_1 and τ_2 values, a discrepancy which may be due to the DSC peak overlap, with the possibility of resulting experimental uncertainty in E_{act}.

5.2. Results for alloy 2124

Kissinger analysis of the DSC GP zone formation peak yielded an activation energy (73.3 kJ/mol) in good agreement with the value from an Arrhenius plot of the rate-averaged isothermal time constant (76.2 kJ/mol). The activation energy for GP zone dissolution is more than twice that for formation but falls in the range of published values for dissolution of GP zones and zone/dislocation complexes [1,6]. E_{act} values from Kissinger analyses of the two DSC precipitation peaks (131 and 114 kJ/mol) are nearly identical to DIC values from τ_1 and τ_2 (128 and 111 kJ/mol) (see Table 1).

Although Kissinger/DSC time constants for GP zone formation agree with those from DIC, agreement

is less good for precipitation. The fact that E_{act} for the fast (low temperature) precipitation process is comparable to that for alloy 2024 suggests that the precipitation processes in the two cases are similar. However, Mishra's TEM studies of 2124 [37] indicate that the low temperature process involves the formation of S' ($CuMgAl_2$), in contrast with the conclusion of Badini et al. [22] that it is due to θ'' ($CuAl_2$). The greater discrepancy of E_{act} values for the slow (high temperature) process in the two alloys makes assignment of a mechanism more problematic. Mishra's TEM study clearly assigns θ' to the second peak, whereas the Badini group conclude that simultaneous formation of θ' and S' phases occurs in 2024. As mentioned above, nucleation processes favor the sequence S' followed by θ'. The temperatures of the second peak for the two alloys differ by only a few degrees (Table 3); consequently differences in the activation energies may be due to slight discrepancies in T_p values.

The maximum exothermic heat released during isothermal GP zone formation (14.7 J/g at ~70°C) is about 1/2 the maximum for precipitation (26.8 J/g at ~270°C). Unfortunately, we are aware of no quantitative models which relate the magnitudes of ΔQ to the amount of precipitation of various species.

Appendix

Table A.1
Parameters for Kissinger fits to scanning experiments

Sample ID	S(°C/min)	T_p(°C)	$1000/T_p$	$\ln(T_p^2/S)$	Fit of Eq. (1) (S<40)
A. GP zone formation		From Eq. (2): $k_0=1.829(+3.08/-1.06)\times10^9$ s^{-1}			
HC6	1.2	45.3	3.1395	15.44	15.39
HC5	2.5	52.8	3.0674	14.75	14.75
HC3	5	60.0	3.0008	14.10	14.17
HC4	10	68.6	2.9259	13.46	13.51
HB13	20	78.8	2.8409	12.83	12.76
HC1	40	91.1	2.7445	12.20	
HC2	80	110.0	2.6098	11.61	
B. *GP zone dissolution*		From Eq. (2): $k_0=5.320$ $(+14.38/-3.88\times10^{14}$ s^{-1}			
HC6	1.2	204.2	2.0944	16.25	16.25
HC5	2.5	212.4	2.0592	15.55	15.50
HC3	5	222.1	2.0191	14.90	14.80
HC4	10	228.5	1.9931	14.23	14.30
HB13	20	238.4	1.9547	13.57	13.56
HC1	40	251.4	1.9062	12.93	
HC2	80	268.7	1.8452	12.30	
C. *1st Precipitation peak*		From Eq. (2): $k_0=3.526$ $(+9.90/-2.61)\times10^{10}$ s^{-1}			
HC6	1.2	235.8	1.9644	16.38	16.30
HC5	2.5	245.7	1.9271	15.68	15.71
HC3	5	256.4	1.8882	15.03	15.10
HC4	10	268.0	1.8476	14.38	14.46
HB13	20	283.5	1.7964	13.74	13.65
HC1	40	310.6	1.7127	13.14	
HC2	80	340.6	1.6293	12.55	
D. *2nd Precipitation peak*		From Eq. (2):$k_0=2.254$ $(+4.33/-1.48)\times10^8$ s^{-1}			
HC6	1.2	252.5	1.9021	16.44	16.35
HC5	2.5	262.5	1.8667	15.75	15.86
HC3	5	278.8	1.8115	15.11	15.11
HC4	10	293.0	1.7662	14.47	14.48
HB13	20	309.4	1.7165	13.83	13.80
HC1	40	319.6	1.6869	13.18	
HC2	80	340.6	1.6293	12.55	

Table A.2
Peak, 2-exponential, and Avrami analyses of isothermal experiments

ID	T/(°C)	$-\Delta Q$/(J/g)	Peak	2-exponential analysis					Avrami Analysis			
			t_{peak}/(min)	α_1/(mW)	α_2/(mW)	τ_1/(min)	τ_2/(min)	r^2 [a]	τ_{rate}/(min)	τ/(min)	n	r^2 [a]
A. *GP zone formation*												
AB11	30	9.82	24.83	0.191	0.589	37.76	38.28	0.99550	38.15	36.71	1.036	0.99731
AA8	40	12.15	6.79	1.725	0.343	12.18	29.83	0.99934	13.50	16.96	0.972	0.99764
AA7	50	14.07	2.54	4.338	0.732	4.911	18.37	0.99966	5.493	8.38	0.946	0.99244
AA6	60	14.24	1.34	10.408	1.418	2.26	9.845	0.99959	2.489	3.96	0.940	0.98939
9H11	60	11.98	1.23	10.810	1.514	2.054	6.723	0.99869	2.245	3.07	0.957	0.99373
9H12	70	14.06	0.74	33.005	3.446	0.849	4.322	0.99942	0.918	1.63	0.912	0.98755
AA13	70	14.47	0.57	24.812	2.911	0.949	4.921	0.99960	1.037	1.76	0.935	0.98596
9H13	80	13.64	0.48	76.844	6.156	0.440	2.456	0.99937	0.469	0.876	0.917	0.98400
AA9	80	13.89	0.39	59.592	5.937	0.470	2.615	0.99946	0.508	0.909	0.939	0.98251
AA10	90	13.38	0.29	117.70	11.379	0.257	1.330	0.99972	0.277	0.607	0.834	0.99017
AA11	100	8.77	0.37	121.71	7.270	0.269	1.588	0.99932	0.282	0.549	0.906	0.98386
B. *Precipitation*												
AB5	220	15.33	26.46	2.247	0.169	16.225	120.0	0.99006				
AB6	230	16.94	12.99	10.015	0.353	5.547	72.61	0.99419				
AB2	240	22.62	6.38	16.710	0.723	3.193	52.701	0.99145				
AB7	250	24.42	3.64	54.351	1.254	1.533	31.25	0.99687				
AB3	260	25.07	2.28	90.767	2.188	1.028	19.45	0.99813				
AB4	270	26.59	1.77	74.336	5.128	0.9537	8.736	0.99791				
AB8	280	25.74	1.07	25.515	8.359	1.573	4.491	0.99913				
AB9	300	24.40	0.55	48.398	3.234	1.293	4.399	0.99977				

[a] r^2 for 2-exponential and Avrami data define goodness of fit of Eqs. (6) and (9) to DIC curves. Generally, r^2 for 2-exponential $\gg r^2$ for Avrami data.

Acknowledgements

The author thanks Jody Hall for fabricating the samples, Raja Mishra for sharing his TEM results, Dick Hall for machining samples to DSC size, Spud Willett for heat treating them, Dan Hayden for computer programs to extract data from the DSC2, and Dusanka Radovic for running DSC7 scans. I greatly appreciate useful discussions with Bill Baxter, Raja Mishra, and Anil Sachdev and am particularly grateful for Bill Baxter's suggestions regarding the manuscript.

References

[1] J.M. Papazian, Met. Trans. 13A (1982) 761.
[2] M. Van Rooyan, J.A. Sinte Maartensdijk, E.J. Mittemeijer, Met. Trans., 19A (1988) 2433. Constraints on heating rate are also discussed in this reference.
[3] C. Antonione, F. Marino, G. Riontino, Mat. Chem. Phys. 20 (1988) 13.
[4] S. Abis, G. Donzelli, J. Mat. Sci. Lett. 7 (1988) 51.
[5] J.M. Papazian, Met. Trans. 19A (1988) 2945.
[6] A.K. Jena, A.K. Gupta, M.C. Chaturvedi, Acta. Metall. 37 (1989) 885.
[7] M.C. Chaturvedi, A.K. Gupta, A.K. Jena, Mat. Sci. Eng. A110 (1989) 187.
[8] M. Van Rooyen, E.J. Mittemeijer, Met. Trans. 20A (1989) 1207.
[9] I. Dutta, D.L. Bourell, Mat. Sci. Eng. A112 (1989) 67.
[10] C. Badini, F. Marino, A. Tomasi, Mater. Chem. Phys. 25 (1990) 57.
[11] A.-M. Zahra, C.Y. Zahra, J. Thermal Anal. 36 (1990) 1465.
[12] C. Badini, F. Marino, A. Tomasi, Mater. Sci. Eng. A136 (1991) 99.
[13] M.J. Starink, P. Van Mourink, Met. Trans. 20A (1991) 665.
[14] M.J. Starink, V. Jooris, P. van Mourink, in: N. Hansen et al. (Eds.), Metal Matrix Composites – Processing, Microstructure and Properties, Risϕ National Lab, Roskilde, Denmark, 1991, p 675.
[15] H.-L. Lee, W.-H. Lu, S.L.-I. Chan, Scripta Met. et Mat. 25 (1991) 2165.
[16] I. Dutta, S.M. Allen, J.L. Hafley, Met. Trans. 22A (1991) 2553.
[17] M.J. Starink, P. van Mourink, Mat. Sci. Eng. A156 (1992) 183.
[18] T.S. Kim, T.H. Kim, K.H. Oh, H.I. Lee, J. Mat. Sci. 27 (1992) 2599.

[19] I. Dutta, C.P. Harper, G. Dutta, Metallurg. Mater. Trans., 25A (1994) 1591. These authors calculated E_{act} for GP zone formation from absolute reaction rate theory; for precipitation they used the method of J.A. Augis, J.E. Bennett, J. Therm. Anal. 13 (1978) 283.
[20] C. Garcia-Cordovilla, E. Louis, J. Narciso, A. Pamies, Mat. Sci. Eng. A189 (1994) 219.
[21] M.P. Thomas, J.E. King, J. Mat. Sci. 29 (1994) 5272.
[22] C. Badini, F. Marino, E. Verne, Mat. Sci. Eng. A191 (1995) 185.
[23] I.N.A. Oguocha, S. Yannacopoulos, Mat. Sci. Eng. A231 (1997) 25.
[24] H.E. Kissinger, Anal. Chem. 29 (1957) 1702.
[25] T. Ozawa, J. Thermal Anal., 2 (1970) 301; 3 (1973) 501; 7 (1975) 601; Bull. Chem. Soc. Japan 57 (1984) 639.
[26] R.L Thakur, in: Advances in Nucleation and Crystallization of Glasses, Am. Ceram. Co., Columbus, 1972, p. 166 (cited in Ref. [29]).
[27] J.A. Augis, J.E. Bennett, J. Therm. Anal. 13 (1978) 283.
[28] E.J. Mittemeijer, L. Cheng, P.J. van der Schaaf, C.M. Brakman, B.M. Korevaar, Met. Trans. 19A (1988) 925.
[29] H. Yinnon, D.R. Uhlmann, J. Non-Cryst. Solids 54 (1983) 253.
[30] J. Sestak, in G. Svehla (Ed.), Comprehensive Analytical Chemistry, Vol. XII, Part D, Elsevier, Amsterdam, (1984), Chap. 9, p 212.
[31] G.W. Smith, Scripta Met. et Mat. 31 (1994) 357.
[32] G.W. Smith, Thermochim. Acta 291 (1997) 59.
[33] G.W. Smith, Thermochim. Acta, 313 (1998) 27.
[34] Preliminary DSC and DIC experiments on samples machined after heat treatment revealed that some GP formation had occurred prior to the calorimetry studies.
[35] M. Avrami, J. Phys. Chem. 7 (1939) 1103; 8 (1940) 212; 9 (1941) 177.
[36] K. Harnisch, R. Lanzenberger, J. Non-Cryst. Solids 53 (1982) 235.
[37] R.K. Mishra (private communication); to be published elsewhere.